RSC Advances

ROYAL SOCIETY OF CHEMISTRY

www.rsc.org/advances

RSC Advances

Functional holey graphene oxide: a new electrochemically transformed substrate material for dopamine sensing

A.B.M. Zakaria,[a] Erick S. Vasquez,[b] Keisha B. Walters,[c] and Danuta Leszczynska[d*]

Increasing active sites through generating holes within the basal plane of graphene sheets is an effective strategy to enhance catalytic performance in various applications such as sensors, electrocatalysis, and electronics. In this study, we report a simple two-step electrochemical approach to convert graphene oxide (GO) into holey graphene oxide (HGO)— graphene sheets with holes ranging from several to tens of nanometers in diameter. The resultant HGO graphene has an order of magnitude more effective surface area than GO, and behaves almost as a reversible electrode system in terms of peak-to-peak seperation value (ΔE) and heterogeneous electron transfer rate constant (k^0) towards the Fe(CN)$_6^{3-/4-}$ redox probe. Characterization of the HGO surface using atomic force microscopy (AFM), transmission electron microscopy (TEM), scanning electron microscopy (SEM), X-ray photoelectron spectroscopy (XPS), Fourier transform infrared spectroscopy (FTIR), Raman spectroscopy, and cyclic voltammetry confirmed generation of holes on the graphene sheets. β-cyclodextrin (β-CD) was immobilized on 'as prepared' HGO demonstrating an additional advantage from the presence of oxygen-containing functional groups on the resultant HGO surface. The β-CD-HGO nanocomposite was investigated as a potential dopamine (DA) sensor material using amperometric techniques. The linear range for DA detection was 0.1-800 μM (N = 3), sensitivity was 4.4 nA/μM cm^2, and the detection limit was 7.6 nM (S/N = 3). In addition to enhanced catalytic performance, HGO can be easily modified with materials such as β-cyclodextrin, as well as nanoparticles, bioactive molecules, and stimuli rersponsive polymers, providing a promising sensor platform.

Introduction

In recent years, graphene has been a material widely investigated across diverse scientific disciplines, both in academic research and technological applications, due to its unique electronic, mechanical and optical properties.[1-3] As a two-dimensional single layer of carbon atoms, the surfaces play a major role in determining its fundamental properties.[4] The most common graphene surfaces are comprised of graphene oxide (GO), a nonconductive hydrophilic carbon material produced from exfoliation of graphite oxide.[5] Hummer's method is widely utilized for large-scale syntheses of graphene oxide,[6] but this method introduces oxygen-containing functional groups—such as epoxy, carboxyl, carbonyl, hydroxyl and ether groups—by disruption of the aromatic lattice in GO in uncontrolled manner.[7] This inevitable introduction of functional groups through over-oxidation

creates defect sites on sp^2 carbon plane of graphene surface and makes GO to be less conductive. To overcome this limitation, researchers have attempted removal of oxygen functional groups from the GO surface and also synthesis of reduced graphene oxide (RGO), a hydrophobic material with large surface area and high conductivity.[8] However, RGO suffers from severe drawbacks limiting its application including the inability to be dispersed in water resulting from the loss of the polar, oxygen-containing functional from the surface.

Recently, considerable focus has been placed on developing unique morphologies of GO by creating oxidative pores within the basal plane of graphene sheets, with the resultant material known as holey graphene oxide (HGO). A unique advantage of HGO is that it has significantly higher catalytic centers due to the increase in edges associated with holes, as compared to GO and RGO. James *et al.* reported a promising strategy where gold nanoparticles (AuNPs) were employed to catalyze the photolytic decomposition of H$_2$O$_2$, thus providing a hydroxyl radical to oxidize RGO, and finally resulting in the production of HGO.[9] Gregg *et al.* demonstrated the enzymatic oxidation of GO and RGO to produce holes on the basal plane of graphitic materials.[10] Recently, Yi *et al.* reported bulk preparation of "holey graphenes" using the deposition of Ag nanoparticles in graphene sheets followed by thermal treatment in air.[11] However, all of these reported methods are complex, requiring a relatively lengthy synthesis timeframes and precise control over reaction and processing parameters.

[a.] Department of Chemistry and Biochemistry, Jackson State University, Jackson, MS 39217, USA.

[b.] Department of Chemical and Materials Engineering, University of Dayton, Dayton, OH 45469, USA.E-mail: evasquez1@udayton.edu

[c.] Dave C. Swalm School of Chemical Engineering, Mississippi State University, Mississippi State, MS 39762, USA. E-mail: kwalters@che.msstate.edu

[d.] Department of Civil and Environmental Engineering, Jackson State University, Jackson, MS 39217, USA .Fax:+1-601-979-3238;Tel:+1-601-979-1091; E-mail: danuta.leszczynska@jsums.edu

† Electronic Supplementary Information (ESI) available: See DOI: 10.1039/x0xx00000x

Hence, there is still a need accurate control over hole formation in the graphene plane using simple, green, and low-cost approaches.

Electrochemical methods are effective ways to modify electronic states by adjusting the electric field to change the Fermi energy level of electrode materials.[12] The inexpensive, time-saving, and environmental friendly characteristics of electrochemical approaches has triggered significant interest in their use to tune the properties of carbon nanomaterials (e.g., carbon nanotubes, graphene) to enhance performance in various applications.[13] For instance, Dhanraj *et al*. reported a remarkable transformation of carbon nanotubes (CNTs) to nanoribbons by a two-step electrochemical approach.[14] Similarly, Zhou *et al.* reported that electrochemically prepared reduced graphene oxide (ERGO) sheets displayed a more conducting nature than those prepared by chemical reduction of graphene sheets.[15] Electrochemical methods provide an effective means for converting GO to a suitable electrode material with large surface area and high conductivity. To gain full advantage of this method depends on the fabrication process for producing thin films of graphene on conducting substrates. For example, self-assembly,[16] spray-coating,[17] spin-coating,[18] direct drop casting of graphene oxide,[19] drop-casting of GO followed by electrochemical reduction,[20] and horizontal-dip coating of GO on indium-tin-oxide[21] are commonly used fabrication methods. Among these methods, self-assembled monolayers (SAMs) are particularly to control the thickness and uniformity of the graphene films.

β-Cyclodextrin (β-CD) is a cyclic oligosaccharide consisting of seven glucose units, that is toroidal in shape with a hydrophobic inner cavity and a hydrophilic exterior.[22] β-CD is a well known biocompatible supramolecule that binds selectively various organic, inorganic, and biological guest molecules in the inner cavity. Moreover, the β-CD hydrophilic exterior preferably attaches with electrophilic functional groups, such as carboxyls and amines, through electrostatic interactions.[23, 24] Therefore, β-CD is a useful probe to evaluate the extent of functional groups on a substrate surface. Dopamine (DA) was chosen as a guest molecule to bind selectively with β-CD to form stable host-guest inclusion complexes. DA is not only an important catecholamine neurotransmitter in the human brain,[25] but is also used as an intravenous medication used to increase heart rate and blood pressure.[26] Therefore, trace level determination of DA in vivo/vitro is important in common medical practice, in determining pathologic states, and in developing future diagnostic methods. Compared to other techniques, electrochemical detection of DA is attractive due to high sensitivity and ease of use.[27-34]

In this paper, we report for the first time a two-step electrochemical method for transforming GO into HGO using electrostatic assembly of GO film onto a 3-aminopropyltrimethoxysilane (APTMS) SAM modified glassy carbon electrode (GCE). The electrochemical approach is an effective way to control geometries and size distribution of holes. We developed a new strategy by exposing the basal plane of graphene oxide and introducing oxidative holes on it

using a cyclic voltammetry-based electrochemical reduction of GO followed by the oxidation of reduced graphene oxide. The GO-, ERGO-, and HGO-modified electrodes were characterized by atomic force microscopy (AFM), transmission electron microscopy (TEM), X-ray photoelectron spectroscopy (XPS), Fourier transform infrared spectroscopy (FTIR), Raman spectroscopy, and cyclic voltammetry. In this study, DA was chosen as a probe to evaluate the electrocatalytic behavior of β-CD modified-electrode materials and to verify the redox reaction-based electrocatalytic performance of β-CD/ HGO nanohybrids.

Experimental

Materials

Graphite powder (300 mesh, 99.5%) was purchased from Alfa Aesar. Sulfuric acid (93-98 w/w %, density 1.84 g/cm³ at 20 °C) was obtained from BDH Chemicals. Other chemicals, $KMnO_4$, H_2O_2 (30%), $NaNO_3$, KCl, 3-aminopropyltrimethoxysilane, $K_3[Fe(CN)_6]$, $K_4[Fe(CN)_6]$, $Na_2HPO_4.7H_2O$, KH_2PO_4, β-cyclodextrin hydrate and dopamine hydrochloride, were purchased from Sigma-Aldrich (USA). All chemicals were analytical grade and were used as received. All stock solutions were prepared using deionized water (18 MΩ.cm) and deoxygenated by purging with ultrahigh pure Ar before starting experiments.

Preparation of GO sheets

GO was prepared by acid oxidation of graphite powder according to the popular modified Hummer's method[6]. Briefly, 2 g of 300 mesh graphite powder, 2 g of $NaNO_3$, and 96 mL of concentrated H_2SO_4 were mixed at 0 °C. A magnetic stirrer (stirring speed, 100 rpm) was continuously used during the entire procedure. Then, 12 g $KMnO_4$ was slowly added to the above mixture while maintaining the temperature at 0 °C. The resultant solution was held at 0 °C for 90 min and then heated at 35 °C for 2 h. To complete the reaction, 200 mL of distilled water was added followed by 10 mL of H_2O_2 (30%) with continued stirring for 10 min to obtain a graphite oxide suspension. Subsequently, the suspension was subjected to high-speed centrifugation at 10,000 rpm for 10 min, repeatedly washed with distilled water until the pH was ~7, and then mild sonication (10 min, 80 W) was used to exfoliate the graphite oxide to obtain a GO suspension. Finally, GO was collected via centrifugation for 5 min at 5000 rpm and then dried in a vacuum oven for 24 h at 90 °C to completely remove the water.

Fabrication of GO/APTMS films on GCE

The GO films were fabricated by a self-assembly method as reported by Zhijuan *et al.*[35] and Chauhan *et al.*[36] Briefly, GO nanosheets were adsorbed on the surface of 3-aminopropyltrimethoxysilane (APTMS)-modified glassy carbon electrodes (APTMS/GCE). As shown in Fig. S1 (ESI†), GCE was preconditioned in 0.5 M H_2SO_4 by cycling ten times at potential window -1.0 to +1.0 V (vs. Ag/AgCl, sat. KCl) at a scan rate of 100 mV/s. Then the activated GCE was immersed in 1% APTMS

anhydrous toluene solution for 15 h allowing the assembly of the APTMS molecules onto the activated GCE surface and reaction via the C-O-Si bond.[36] After being washed with copious amounts of anhydrous toluene and dried in ambient air, this APTMS-modified electrode was dipped in a GO aqueous solution (1 mg/mL) for 4 h. Thus GO was self-assembled onto the APTMS-modified GC electrode via electrostatic interaction between the positively charged amine groups on the SAM terminus and negatively charged carboxyl groups present on the GO. This electrode, termed as GO/APTMS/GC electrode, was electrochemically reduced followed by oxidation of the reduced graphene oxide in 0.5 M H_2SO_4. The resulting electrochemically reduced and oxidized electrodes are termed as ERGO/APTMS/GC and HGO/APTMS/GC, respectively. Fig. 1 presents a schematic representation for the modification of GCE.

Preparation of the β-CD modified graphene electrodes

β-CD modified electrodes were prepared according to the process reported elsewhere.[37] In brief, the deposition of a self-assembled monolayer of β-CD over the different surface-modified graphene electrodes described previously was carried out by immersion into a 1.0 mM aqueous solution of β-CD for 12 h at room temperature. Electrodes were then washed using ultrapure water to remove the non-adsorbed β-CD molecules on the electrode surface. The resulting modified electrodes are termed as β-CD-GO/APTMS/GC, β-CD-ERGO/APTMS/GC and β-CD-HGO/APTMS/GC.

Characterization

The electrochemical measurements were carried out with a CHI 440 electrochemical analyzer (CH Instruments, Austin, TX, USA), using a conventional three-electrode system. The glassy carbon electrode (GCE, 3mm diameter), Ag/AgCl/saturated KCl (Model CH111, CH Instruments, Austin, TX, USA), and a platinum wire were used as working, reference, and counter electrodes respectively. All experimental solutions were deoxygenatede for 20 min using high purity argon and maintained under argon atmosphere during measurements. FT-IR spectra were collected on a Thermo Nicolet Model Nexus 870 FT-IR spectrometer over a 400 to 4500 cm^{-1} wavenumber range with DTGS or MCT detector. Raman spectroscopic measurements were carried out using a continuous wavelength DPSS laser from laser glow technology (LUD-670) operating at 670 nm as an excitation light source. An InPhotonics 670 nm Raman fiber optic probe was used for excitation and data collection. It is a combination of 90 µm excitation fiber and 200 µm collection fiber with filtering and steering micro-optics. A miniaturized QE65000 scientific-grade spectrometer from Ocean Optics was used as the Raman detector, with a 220-3600 cm^{-1} spectral response range. It was equipped with TE-cooled 2048 pixel CCD and interfaced to computer via a USB port. X-ray photoelectron spectroscopy (XPS) was performed with a Mg Kα X-ray source (300 W, 15 kV) and a 45$^{°}$ take-off angle. An Omni Focus II small-area lens and a PHI 10-360 spherical capacitor energy analyzer were used for data acquisition. Survey and high-resolution spectra were

collected using a minimum of 10 scans with a 26.95 eV pass energy across the 1100 to 0 eV range and a minimum of 15 scans with a 23.5 eV pass energy with a 0.1 eV step size, respectively. For XPS analysis, electrode materials were deposited onto UV/O-treated, Au-coated Si wafers and allowed to dry inside a ventilated hood for 24 h. Spectra from a minimum of three areas on each sample were used for XPS analyses. Gaussian peak fitting was performed using CasaXPS software v.2.2.88, and average results are reported. Transmission electron microscopy (TEM) was performed using a JEOL-2100F transmission electron microscope operated at 100 kV. For TEM analysis, sample droplets were placed on Cu grids (Electron Microscopy Science) and the solvent allowed to evaporate at ambient temperature inside a ventilated hood. AFM data was collected with a Dimension Icon operated in ScanAsyst and tapping modes. Bruker's PeakForce KPFM probes with a 300 kHz resonance frequency, 42 N/m spring constant, and 2 nm sharp tip were used for all AFM measurements. For AFM imaging, the GC electrode samples were dispersed into water by ultrasonication for 20 min. Then ~ 10 µL of the dispersed sample was drop casted onto freshly cleaned Si wafers, spin-coated at 1000 rpm and allowed to dry under ambient conditions for 30 min prior to imaging. SEM images were taken using a ZEISS Supra 40 VP scanning electron microscope (SEM) on samples 'as formed' on the GC electrodes. Note that the data for multiple measurements (n=3) on five independently prepared electrode samples indicates that process was very repeatable, and the electrode modifications was relatively homogeneous.

Fig. 1

Results and discussion

Investigation of two-step electrochemical treatment of GO/APTMS/GC electrode

Fig. 1 represents the fabrication of GO, followed by a two-step electrochemical process for preparing holey graphene oxide (HGO). For the first step (Step-1), electrochemical reduction of the obtained GO/APTMS/GC electrode was conducted by cyclic voltammetry (CV) over the potential range from 0.0 to -1.2 V vs. Ag/AgCl (3M KCl sat.) in 0.5 M H_2SO_4 at scan rate of 50 mV/s (Fig. 2A). A large cathodic current peak at -1.0 V appeared during the first cycle which might be due to the reduction of oxygen-containing functional groups (epoxy, carboxyl, carbonyl and hydroxyl) on the GO surface. During the second cycle, the reduction peak current almost vanished, but the reduction current at switching potential at -1.2 V increased sharply for several cycles (7 cycles, see Fig. S2, ESI†). With further cycling, this reduction current decreased gradually, and stabilized after 30 cycles. The final cycle is shown by the black line in Fig. 2A, and indicates a complete reduction of oxygen-containing functional groups on GO surface.

Fig. 2

For the second step (Step-2) of the treatment, just after finishing the cathodic cycle, an anodic scan was run starting over the potential window from -0.2 to +1.2 V vs. Ag/AgCl at scan rate 50mV/s in 0.5M H_2SO_4 (Fig. 2B). In the first cycle, the CV shows a huge oxidation peak that appeared at +0.4 V potential in the forward scan, and a weak peak appeared at +0.2 V in the backward scan. This result indicates the introduction of oxygen-containing functional groups on the graphene surface that could not be reduced in reverse scan within the applied potential range. In the second cycle, the redox peak was completely different; the intensity of the oxidation peak was decreased and shifted to around +0.35 V in the forward scan, but it was not shifted in the reversed scan. With further cycling, intensity of the oxidation and the reduction peak at +0.35 V and +0.2 V, respectively, increased gradually. The oxidation peak at +0.35 V indicates the introduction of a new oxygen-containing functional group, different than the one related to the +0.4 V peak seen in the first cycle. Moreover, this functional group at +0.35 V could be reduced at +0.2 V. On the other hand, in the first cycle, the reduced peak appearance at +0.2 V suggests that the introduction of the functional group at +0.35 V may be dominated by the one at +0.4 V. In addition, we observed that the oxidation edge current was decreasing, and then remained constant after 15 cycles (the final cycle is in black line, Fig. 2B). This result suggests that from the 2nd to the 15th cycle, a redox active oxygen containing functional group, as for example, the quinone-like groups can be reduced to hydroquinone and oxidized back reversibly. Moreover, the redox active oxygen was gradually attached on the graphene surface, reaching the maximum level.[38]

The electrochemical phenomena displayed by these modified graphene surfaces suggest the following:

1) The self-assembly method favors the formation of a single or very few layers of graphene oxide. Oxygen-containing functional groups, especially carboxyl groups on the edge carbon, were mostly occupied by amine functionalities attached to the APTMS linker.[39] Therefore, only basal carbon on graphene sheets were available for both electrochemical reduction and oxidation.

2) In the first step, the oxygen surface functional groups participated in a reduction as demonstrated by a huge reduction peak at the first scan (Fig. 2A, red line). After successive reduction scans, the graphene surface was uniformly functionalized mostly by hydroxyl groups, as further discussed in the XPS and FTIR sections, resulting from the transformation of oxygen functional moieties present in carboxyl, carbonyl, and epoxide groups. As reported elsewhere,[40] epoxy groups which are found predominately at the basal plane, are more stable than carboxyl and carbonyl groups. Therefore, breaking the epoxy bond (C-O) groups possibly requires additional cycle runs. It is suggested that the 1st reduction cycle favors the conversion of carboxyl and carbonyl to the corresponding hydroxyl groups having lower energy barrier, and then cycles 2 to 30 contribute higher energy to meet the large energy barrier conversion of epoxy to hydroxyl groups. This phenomenon might vary based on the quality of graphene oxide in terms of their defects such as impurities (carbonaceous and metallic), thickness, and homogeneity of the coating. Moreover, the resultant single layer (or few layers) of reduced graphene oxide might have distorted benzene rings after losing the oxygen containing functional group on ring carbon.[8] Indeed, wavy-silk GO was transformed to a surface of high density wrinkles, folds and rolled edges (SEM image of reduced GO, see Fig. S3, ESI†). In addition, the edge-plane-like defective sites were created on the basal plane of reduced graphene sheets, making the surface more sensitive to the next attack by anodic oxidation.

3) In the second step, the vulnerable single layer (or few layers) of reduced graphene oxide was exposed to the surrounding active oxygen ($O_2 + 2H^+ + 2e \rightarrow H_2O_2$ created during cathodic scan and SO_3H^- from H_2SO_4) at the close vicinity of the electrode surface.[41-43] These active oxygen species can possibly break the distorted C-C single bond of the benzene ring (where each carbon is bonded with either hydroxyl or oxygen of another epoxy group) on the graphene sheet creating holes on the graphene oxide surface. This observation is also consistent with previously reported epoxy chain-induced unzipping of carbon rings.[44-46] It is also suggested that once a hole has been initiated, it will continue until relieved by the benzene ring bond-angle strain, adjusting the regular energy distribution across the planar graphene sheets. GO after the electrochemical process was characterized using morphologic and spectroscopic characterizations, as described next.

Fig. 3

Surface Morphology Characterization

The surface morphology and structure of exfoliated GO, ERGO and HGO were investigated using atomic force microscopy (AFM), scanning electron microscopy (SEM) and transmission electron microscopy (TEM). Fig. 3 shows the atomic force microscopy of the exfoliated GO and HGO. As shown in Fig. 3A, the exfoliated GO sheets were flat, nonporous and straight edges with an average thickness of about 1.6 nm (see Fig. S4, ESI†). On the other hand, the thickness of the ERGO and HGO was about 2.7 and 3.6 nm, respectively (Fig. 3B and Fig. S4, ESI†). In this case, the thickness was increased due to the APTMS linker attached on the backside of ERGO and HGO sheets. After electrochemical reduction of GO, the resultant surface became smooth compared to that of GO. This difference was clearly observed using the height profiles along the cross section lines of the corresponding surfaces (Fig. S4, ESI†). More importantly, the HGO edges are no longer straight and pores, with diameters ranging from a few nanometers to several hundred nanometers, are randomly distributed across the entire sheets due to oxidation of the reduced form of graphene oxide.

Fig. 4

Fig. 4 (A, B, C and D) contrast the resulting surface features of GO following electrochemical transformation to HGO. According to the SEM and TEM observations, the wavy-silk GO was changed into HGO displaying a flat graphene surface with holes. Fig. 4E,F show the nanohybrids of β-CD with GO and HGO respectively. In TEM image of β-CD/GO (Fig. 4E), we observed that β-CD was selectively anchored with edge carbon functional group mostly carboxyl (hydrophilic character) rather than that of basal carbon mostly hydroxyl group (hydrophobic character) of graphene sheet. Conversely, in HGO (Fig. 4F), β-CD was randomly immobilized on the graphene sheet due to increasing edge associated hydrophilic functional group (carboxyl) across the entire sheet.

Fig. 5

Spectroscopic Characterization

In order to confirm the oxidative holes on graphene plane and changes in the functional groups attached to the different graphene surfaces (GO-, ERGO- and HGO-modified substrate), we carried out X-ray photoelectron spectroscopy (XPS), Fourier transform infrared spectroscopy (FTIR), and Raman spectroscopy analyses. Fig. 5A shows the XPS survey spectra for the GO/APTMS/GC, ERGO/APTMS/GC and HGO/APTMS/GC substrates. All substrates show two major peaks, at 285.0 and 531.6 eV, that correspond to C 1s and O 1s, respectively. Other minor peaks at 398, 154, and 104 eV were assigned to N 1s, Si 2s and Si 2p respectively.[47] Interestingly, for exfoliated GO only, N and Si peaks were not observed (Fig. S5, ESI†). This result suggests the successful attachment of GO on GC electrode through the amine functionality of the APTMS linker. Moreover, the C/O ratio of both GO (with and without APTMS) were similar, suggesting GO/APTMS could be considered as a representative of GO material for comparing ERGO and HGO-substrate materials (see Table 1). After electrochemical reduction of GO-modified substrate, the C/O intensity ratio (Fig. 5A, curve b) increased from 2.09 to 4.14 indicating the removal of surface oxygen functional groups from GO.[12] Furthermore, after electrochemical oxidation of the reduced form of GO, the intensity ratio C/O was decreased from 4.14 to 1.84 indicating the introduction of oxygen functional group on the graphene surface. These results are consistent with previous reports, and confirm the overall two-step electrochemical reduction and oxidation treatment.[48]

Table 1
Fig. 6

Additionally, Table 1 shows the atomic percentage of carbon and oxygen in different substrate materials. Different types of carbon and oxygen functional groups were also confirmed by C 1s and O 1s XPS high resolution scans. The high resolution C 1s spectrum of GO substrate in Fig. 5B shows four peaks at 285.0, 285.8, 287.4 and 288.8 eV, corresponding to C-C sp^2 carbon, C-O bond, C=O bond and HO-C=O bond, respectively.[49-51] As is well-known, the binding energy of 287.4 eV for C=O is similar to that of C-N, and hence a separate C-N peak was not observed in all substrate spectra.[52, 53] After electrochemical

reduction, the C 1s spectrum of ERGO/APTMS/GC substrate in Fig. 5C shows three peaks at 285.0, 286.0, and 288.2 eV corresponding to the C-C sp^2 carbon, C-O bond and C=O bond respectively. In this spectrum, the intensities of oxygen-containing functional groups were lower compared to GO-modified substrate. Conversely, four C 1s (sp^2 carbon, C-O, C=O and HO-C=O) peaks with high intensity of different oxygen functional groups were re-observed at the C 1s spectrum of HGO/APTMS/GO substrate (Fig. 5D). High resolution XPS spectra of O 1s in Fig. 6 (C-O at 531.8 eV, C=O at 533.8 eV and HO-C=O at 534.8 eV) also follows this trends.[54] In particular, after electrochemical oxidation, the intensities of oxygen functional groups HO-C=O and C=O were obviously increased as compared to that of GO-modified substrate, and the overall oxygen content was found to increase to 16.0 at.%. This result indicates that higher edge carbon associated with holes on graphene sheet facilitates the formation of higher carboxyl functional groups at HGO-modified substrate.

Fig. 7

Further analysis using the FTIR transmittance spectra (KBr) were performed on (a) GO-, (b) ERGO-, and (c) HGO-substrates (Fig. 7) to carefully study the oxidation level and chemical functionalities of different graphene surfaces. The spectrum of HGO illustrates high absorption of O-H group in the regions of O-H (500-900 cm^{-1} and 3000-3700 cm^{-1}) and C=O modes (1700-1750 cm^{-1}) and lower absorption in the regions of C=C-H (800-1000 cm^{-1}) and C-O modes (1000-1250 cm^{-1}). When GO was electrochemically reduced, the C=O vibration band almost disappeared, the broad O-H and C-O stretching bands remained, and C=C-H band was newly appeared. It suggests the optimal reduction of GO surface with some degree restoration of C=C bonding result in a high pure graphene surface. While ERGO was re-oxidized electrochemically, the spectrum of HGO exhibited a stronger IR absorption by C=O and C-O modes compared to GO. The most striking contrast was observed in the HGO spectrum with the large growth of two broad -OH absorption bands in regions 500-1000 and 3000-3700 cm^{-1} compared to both RGO and GO spectra. This observation implies that electrochemical oxidation of ERGO alleviates a build-up of O-H groups on RGO sheets possibly providing a pathway for further oxidation, resulting in the formation of holes on graphene sheets.

Fig. 8

Lastly, we employed Raman spectroscopy as a widely used nondestructive technique to characterize ordered and disordered crystal structures of carbon nanomaterials. We used spectroscopic probe to investigate the structural changes of graphene carbon networks due to reduction/oxidation of surface functional groups during the electrochemical process. The Raman spectrum of the pristine graphite has been reported to display a strong G band at 1579 cm^{-1}, a weak D band at 1360cm^{-1}, and a middle 2D and D+ D$^/$ bands at 2700 cm^{-1} and 2940 cm^{-1} respectively.[55] In Fig. 8, the D and G bands

of GO/APTMS/GC (curve b) substrate spectrum were broadened and shifted at positions 1365 cm^{-1} and 1607cm^{-1}, respectively, due to the severe defects resulting from oxidative exfoliation of pristine graphite (curve a). After completing reduction cycles, in ERGO/APTMS/GC substrate, a clear spectrum (Fig. 8, curve c) with sharp D and G bands was observed at 1338 cm^{-1} and 1620cm^{-1}, respectively. It suggests that the order of graphene carbon in-plane sp^2 domain is partly recovered during the electrochemical reduction that is consistent with previous reports.[56] The intensity ratio of D and G bands (I_D/I_G) of carbon materials is usually assigned to demonstrate the extent of surface modification or defects arising from distortion, vacancies and edges of hexagonal network of carbon atoms.[57] As shown in Fig. 8, the intensity ratio (I_D/I_G =1.23) for ERGO-modified substrate is higher than that of GO (I_D/I_G =0.91). This observation is attributed to the increased defect concentration present in ERGO relative to that in GO. Moreover, in ERGO-substrate, a broad and weak 2D and D+D$'$ band at 2652 cm^{-1} and 2928 cm^{-1}, respectively, was observed due to the hydrogenation of graphene surface.[58] Then, after running anodic cycles the intensity of both D and G bands was decreased comparing to that in ERGO-modified substrate but similar to the peaks observed for GO-modified substrate. But in this case, the intensity ratio (I_D/I_G=1.01) of HGO/APTMS/GC substrate is higher than that in GO-modified substrate. In addition, there is a significant change in 2D and D+D$'$ bands. The weak and broadened 2D and D+D$'$ bands of ERGO-modified substrate were completely disappeared in HGO-modified substrate spectrum. The results are consistent with prior literature findings[10, 59] suggesting that the decreased intensity ratio and significant change in 2D and D+D$'$ bands of HGO- comparing to ERGO-substrate are due to the introduction of oxygenated functionalities that disrupt the planar sp^2 structure, resulting in cracks or holes on the graphene surface. The peak assignments for Raman spectra and XPS are summarized in Table S1 (ESI†).

Fig. 9

Electrochemical characterization
We employed cyclic voltammetry (CV) of [Fe(CN)$_6$]$^{3-/4-}$ redox probe to investigate the intrinsic electron transfer properties of the obtained holey graphene oxide (HGO) and compared its electrochemical behavior with GO- and ERGO-modified electrodes. Fig. 9A shows the electrochemical responses of bare GC, GO/APTMS/GC, ERGO/APTMS/GC and HGO/APTMS/GC electrodes to argon saturated 1.0 mM K$_3$[Fe(CN)$_6$]/K$_4$[Fe(CN)$_6$] (1:1 molar ratio) in 1.0 M KCl electrolyte. All the electrodes show well-defined peaks in the forward and reverse scans due to the oxidation and reduction of [Fe(CN)]$^{3-/4-}$ redox couple. In all cases, the anodic (I_{pa}) and cathodic (I_{pc}) peak currents are varied linearly with respect to the square root of scan rate ($v^{1/2}$), indicating that the electrode kinetics are controlled by mass transport (semi-infinite linear diffusion) of the reactant (Fig. 9B). This criteria of electrode surface is followed by the Randles-Sevcik equation (Eqn. 1),[60]

$$I_p = 2.687 \times 10^5 ACn^{3/2}(Dv)^{1/2} \qquad (1)$$

where I_p is the peak current (A), A is the electroactive area (cm^2), C is the concentration of electroactive species (cm^3/mol), n is the number of electrons taking part in the redox, D is the diffusion coefficient (cm^2/s) and v is the scan rate (V/s). In equation 1, the peak current is directly related to the scan rate and the effective surface area (ESA) of electrode for a particular electrochemical redox system. Using the above equation, the effective area of the electrodes was calculated to be 0.065, 0.012, 0.249 and 0.194 cm^2 for bare GC, GO/APTMS/GC, ERGO/APTMS/GC and HGO/APTMS/GC, respectively (see Table S2, ESI†). Comparing with geometric area of bare GC electrode (0.07cm^2), the estimated value of effective surface area 0.065 ± 0.005 cm^2 indicates the redox reactions occurred predominantly on a clean electrode surface. The lowest and highest ESA were observed in GO- and ERGO-modified substrates, respectively. It suggests that the minimum and maximum active sites (exposed edges) were accessible to the [Fe(CN)$_6$]$^{3-/4-}$ redox couple. In case of HGO-substrate, the ESA was smaller than ERGO- and 1-order of magnitude higher than GO-substrate. It indicates that the active sites created on ERGO- might not be fully exposed to the probe ions in case of HGO-substrate due to the insulating effect of adding oxygen containing functional group on edge carbon created during oxidation (step-2, anodic scan) of the reduced graphene surface. Moreover, other two important parameters, electron transfer rate constant (k^o) and peak-to-peak separation value (ΔE) also follow this trend. The electron transfer rate constant (k^o) was calculated using Nicholson's working curve (see section S5). The calculated k^o value, 0.045 ± 0.002 for GO-substrate, is consistent with a previous report.[61] As shown in Table S2, after electrochemical reduction, the k^o value was decreased possibly due to losing electroactive particulates anchored on carbonaceous debris that were attached with mother GO-substrate by π-π interaction and thus the surface being a true monolayer in nature.[62, 63] Again after electrochemical oxidation of the ERGO- substrate, the k^o value became lower due to the oxygen containing functional group increase on HGO- substrate surface. This observation is true with other CV parameters. According to the CV measurements, the ΔE value and the anodic and cathodic peak ratio (I_{pa}/I_{pc}) of both ERGO- and HGO-modified electrodes showed 61 mV and close to 1 respectively at scan rate 100 mV/s which are nearly reversible Nerstian behavior with the theoretical value of 59mV for one-electron transfer process.[64] Since the ΔE value is directly correlated to the electron transfer kinetics, the fastest electron transfer electrochemical reaction could be possible at both ERGO- and HGO-modified electrodes. In Fig. 9B, we also observed that the anodic and cathodic peak current of HGO- was not completely linear at higher scan rate comparing to ERGO- substrate electrode. It suggests that HGO- is not fully reversible with the redox probe at higher scan due to the possibility of absorbing the redox probe ion on its surface.[65] It indicates that the presence of surface active functional groups may interact and stabilize the

RSC Advances Accepted Manuscript

probe ion. As a summary, the above evidences suggest that the HGO-substrate electrode has a faster electron transfer kinetics than the GO-substrate and the bare GC, but a little lower than the ERGO-substrate electrode possibly due to the additional active sites with oxygen containing functional groups resulting from holes on graphene plane.

Fig. 10

Electrochemical catalysis of dopamine (DA) on different electrodes modified by β-cyclodextrin (β-CD)

To further evaluate the practical application of HGO in the field of electrochemical sensors, we also examined the nanocomposite of β-cyclodextrin (β-CD) with HGO modified electrode, and its electrocatalytic activity toward dopamine (DA) sensing. Since a large number of active sites containing polar groups (mostly carboxyl) have been developed on HGO surface, large amounts of β-CD could be immobilized on the surface due to the hydrophilic interactions with the exterior hydroxyl groups of β-CD. Moreover, the prepared β-CD modified HGO electrode could serve as a sensitive and selective platform by forming an inclusion complex with the dopamine molecule via hydrogen bonding interactions, which might increase the response of the sensor.[66] Fig. 10 shows cyclic voltammograms (CVs, 1st cycle) of DA (1.0 mM) in phosphate buffer solutions (PBS 0.1M, pH 7.40) at scan rate 50mV/s on β-CD-GO/APTMS/GC (curve a), β-CD-ERGO/APTMS/GC (curve b), HGO/APTMS/GC (curve c), bare GCE (curve d), and β-CD-HGO/APTMS/GC (curve e).

It is well known that there are four DA oxidation/reduction peaks that correspond to the reactions shown in Scheme 1.[67, 68]

Scheme1

The most obvious observation from Fig. 10 is that the highest two pairs of oxidation/reduction peak currents corresponding to above four reactions of DA were at β-CD-HGO/APTMS/GC among all other modified electrodes, indicating a favorable catalytic activity of β-CD/HGO towards the oxidation/reduction of this compound. It was also observed that the double layer capacitance at β-CD/HGO is much higher when compared to only HGO modified electrode (curve c: dotted line), which means that β-CD provides a much higher electrochemical active area for enhanced electrochemical response toward DA. As shown in Fig. 10e, the voltammogram displays anodic peak at 0.182 V vs. Ag/AgCl and a cathodic peak at 0.142 V vs. Ag/AgCl corresponding to the oxidation of DA to o-dopaminoquinone (DAQ) and the reduction of DAQ back to DA, respectively (equation 1). At pH 7.4, DAQ undergoes intramolecular cyclization through deprotonation of the amino group to form leucodopaminochrome (LDAC) (equation 2). Thus, a redox pair with a cathodic peak at -0.273 V vs. Ag/AgCl and an anodic peak at -0.229 V vs. Ag/AgCl are assigned to the redox couple LDAC/dopaminochrome (DAC) (equation 3). We need to mention that the anodic peak at -0.229 was not

observed as it was not yet formed in the first cycle (Fig. S6, ESI†).

On the other hand, for the β-CD-GO/APTMS/GC, β-CD-ERGO/APTMS/GC, HGO/APTMS/GC, and bare GC electrodes, the CV scan displays an anodic peak at 0.304, 0.184, 0.204, 0.213 V and a cathodic peak at 0.066, 0.128, 0.119, 0.067 V assigning to the DA/DAQ redox couple shown in Fig. 10 a, b, c and d respectively. Both (anodic and cathodic) peak currents for β-CD/ERGO, only HGO, and β-CD/GO nanohybrid electrodes were much smaller than that of the β-CD/HGO electrode. Moreover, β-CD/GO showed anodic peak potential shift toward more positive as compared to the peak of β-CD/ERGO and only HGO electrode. In addition, the oxidation peak current of DA was enhanced at bare GC electrode comparing to β-CD/ERGO, only HGO and β-CD/GO. Besides, the DA/DAQ redox peak difference ΔEp for β-CD/GO, β-CD/ERGO, only HGO and bare GC were 0.259, 0.09, 0.082 and 0.147V, respectively, while the β-CD/HGO electrode was 0.04V. All observations suggest that β-CD was not properly anchored due to the hydrophobic surface interaction with ERGO/APTMS/GC and the limited anchoring through hydrophilic interaction along the edges (as shown in TEM image Fig. 4E) of GO/APTMS modified GC electrode. In contrast, HGO favors β-CD molecules immobilized on its surface providing high density of active sites resulting enhanced electrocatalytic activity toward DA when compared to all other electrodes.

Fig. 11

Amperometric response of DA at the β-CD-HGO/APTMS/GC electrode

In order to determine the linear range and sensitivity of the prepared β-CD-HGO/APTMS/GC electrodes for DA detection, amperometric responses are displayed in Fig. 11A. The response currents were monitored at an applied potential fixed at 0.200 V after successive additions of DA into 0.1M PBS (pH 7.40). Fig 11C shows the linear response of the oxidative current density against the corresponding DA concentration for this electrode. The linear regression equation was I ($\mu A/cm^2$) = 0.0044c (μM) + 0.1204, with a correlation coefficient of 0.9907. From the slope of 0.0044 $\mu A/\mu M.cm^2$, the detection limit was estimated to 7.6 nM (S/N=3) using the following method: limit of detection, LOD = $SD_{background}/S$, where S= slop or sensitivity, SD=standard deviation. The linear range of the β-CD-HGO/APTMS/GC was 0.1-800 µM while the sensitivity to the oxidation of DA was 4.4 nA/µM.cm². The comparison of β-CD-HGO/APTMS/GC with other DA sensor previously reported is demonstrated in Table 2. This electrode shows better linearity range and detection limit than other modified electrodes.

Table 2

Stability, Reproducibility, and anti-interference property of the β-CD-HGO/APTMS/GC electrode

Since the electrode preparation method is simple and rapid, it is not so important for the electrode to be stable over a long period of time. However, this β-CD-HGO/APTMS/GC electrode results in higher stability for amperometric measurement at a constant potential. Fig. 11B displays the stability of the response without DA in 0.1 M PBS (pH 7.40) at an applied potential of 0.200 V. The response remains stable throughout 1 hour. We also evaluated the reproducibility by measuring amperometric (E_{ap}= 0.2) responses of the five separately prepared β-CD-HGO/APTMS/GC electrodes in pH 7.4 with sequential addition of 0.1 mM of DA in 0.1 M PBS. The test result was shown in Table S3 (ESI†). The relative standard deviation (R.S.D) was 6.1% suggesting the high reproducibility of the preparation method of this modified electrode. Moreover, Fig. 11D shows the amperometric response of β-CD-HGO/APTMS/GC investigated in pH 7.4 PBS with sequential additions of 0.05 mM DA and potential interferents including uric acid (UA) and ascorbic acid (AA) of 0.1 mM for each addition. A well-defined DA response was obtained and insignificant responses were observed for interfering species. The observation suggests that this electrode shows good selectivity for DA detection.

Conclusions

In summary, we have developed an unprecedented method of generating holes on basal plane of graphene oxide (GO) by a complete electrochemical method with reduction followed by oxidation of GO. The current limitations of chemically synthesized holey graphene oxide (HGO), due to over-oxidation and defects of the graphene surface, could be eliminated by using controlled-potential-step experiments as demonstrated in this study. The as-synthesized HGO exhibited high active surface area, high electron transfer, and good chemical stability, as well as being an attractive platform for electrode modification. Particularly, the β-CD-HGO nanohybrid produced using electrochemically-generated HGO showed much higher electrocatalytic activity for the oxidation of dopamine than that of β-CD-GO and β-CD-ERGO. This finding implies that the presence of oxygen functionalities in conjugation with additional edges associated with holes in HGO may contribute to the SAM decoration of other nanomaterials or bio-molecules by a defect-mediated nucleation, and lead to formation of an enhanced electrochemical platform for constructing efficient biosensing, biomedical, energy conversion systems. This trait could open a new horizon in nanoelectronics, supercapacitors, solar cells and sensor devices.

Acknowledgements

References

1. A. K. Geim and K. S. Novoselov, *Nat Mater*, 2007, **6**, 183-191.
2. M. Pumera, *Chemical Society Reviews*, 2010, **39**, 4146-4157.
3. J. Shen, Y. Hu, C. Li, C. Qin and M. Ye, *Small*, 2009, **5**, 82-85.
4. V. Georgakilas, M. Otyepka, A. B. Bourlinos, V. Chandra, N. Kim, K. C. Kemp, P. Hobza, R. Zboril and K. S. Kim, *Chemical Reviews*, 2012, **112**, 6156-6214.
5. D. C. Marcano, D. V. Kosynkin, J. M. Berlin, A. Sinitskii, Z. Sun, A. Slesarev, L. B. Alemany, W. Lu and J. M. Tour, *ACS Nano*, 2010, **4**, 4806-4814.
6. W. S. Hummers and R. E. Offeman, *Journal of the American Chemical Society*, 1958, **80**, 1339-1339.
7. A. Lerf, H. He, M. Forster and J. Klinowski, *The Journal of Physical Chemistry B*, 1998, **102**, 4477-4482.
8. S. Mao, H. Pu and J. Chen, *RSC Advances*, 2012, **2**, 2643-2662.
9. J. G. Radich and P. V. Kamat, *ACS Nano*, 2013, **7**, 5546-5557.
10. G. P. Kotchey, B. L. Allen, H. Vedala, N. Yanamala, A. A. Kapralov, Y. Y. Tyurina, J. Klein-Seetharaman, V. E. Kagan and A. Star, *ACS Nano*, 2011, **5**, 2098-2108.
11. Y. Lin, K. A. Watson, J.-W. Kim, D. W. Baggett, D. C. Working and J. W. Connell, *Nanoscale*, 2013, **5**, 7814-7824.
12. H.-L. Guo, X.-F. Wang, Q.-Y. Qian, F.-B. Wang and X.-H. Xia, *ACS Nano*, 2009, **3**, 2653-2659.
13. Y. Shao, J. Wang, M. Engelhard, C. Wang and Y. Lin, *Journal of Materials Chemistry*, 2010, **20**, 743-748.
14. D. B. Shinde, J. Debgupta, A. Kushwaha, M. Aslam and V. K. Pillai, *Journal of the American Chemical Society*, 2011, **133**, 4168-4171.
15. M. Zhou, Y. Wang, Y. Zhai, J. Zhai, W. Ren, F. Wang and S. Dong, *Chemistry – A European Journal*, 2009, **15**, 6116-6120.
16. X. Zhou, X. Huang, X. Qi, S. Wu, C. Xue, F. Y. C. Boey, Q. Yan, P. Chen and H. Zhang, *The Journal of Physical Chemistry C*, 2009, **113**, 10842-10846.
17. S. Gilje, S. Han, M. Wang, K. L. Wang and R. B. Kaner, *Nano Letters*, 2007, **7**, 3394-3398.
18. E. Shi, H. Li, L. Yang, L. Zhang, Z. Li, P. Li, Y. Shang, S. Wu, X. Li, J. Wei, K. Wang, H. Zhu, D. Wu, Y. Fang and A. Cao, *Nano Letters*, 2013, **13**, 1776-1781.
19. G. P. Keeley, A. O'Neill, M. Holzinger, S. Cosnier, J. N. Coleman and G. S. Duesberg, *Physical Chemistry Chemical Physics*, 2011, **13**, 7747-7750.
20. H. Imran, P. N. Manikandan and V. Dharuman, *RSC Advances*, 2015, **5**, 63513-63520.
21. H. G. Jeon, Y. H. Huh, S. H. Yun, K. W. Kim, S. S. Lee, J. Lim, K.-S. An and B. Park, *Journal of Materials Chemistry C*, 2014, **2**, 2622-2634.
22. R. Freeman, T. Finder, L. Bahshi and I. Willner, *Nano Letters*, 2009, **9**, 2073-2076.
23. A. González-Campo, S.-H. Hsu, L. Puig, J. Huskens, D. N. Reinhoudt and A. H. Velders, *Journal of the American Chemical Society*, 2010, **132**, 11434-11436.
24. C. Feng, G. Lu, Y. Li and X. Huang, *Langmuir*, 2013, **29**, 10922-10931.
25. R. M. Wightman, L. J. May and A. C. Michael, *Analytical Chemistry*, 1988, **60**, 769A-793A.

RSC Advances Accepted Manuscript

26. J. P. Long, S. Heintz, J. G. Cannon and J. Kim, *Journal of Pharmacology and Experimental Therapeutics*, 1975, **192**, 336-342.

27. L. A. Mercante, A. Pavinatto, L. E. O. Iwaki, V. P. Scagion, V. Zucolotto, O. N. Oliveira, L. H. C. Mattoso and D. S. Correa, *ACS Applied Materials & Interfaces*, 2015, **7**, 4784-4790.

28. G. Fabregat, E. Armelin and C. Alemán, *The Journal of Physical Chemistry B*, 2014, **118**, 4669-4682.

29. S. M. Ghoreishi, M. Behpour, S. Mousavi, A. Khoobi and F. S. Ghoreishi, *RSC Advances*, 2014, **4**, 37979-37984.

30. Y. Huang, Y.-E. Miao, S. Ji, W. W. Tjiu and T. Liu, *ACS Applied Materials & Interfaces*, 2014, **6**, 12449-12456.

31. T.-H. Tsai, S. Thiagarajan, S.-M. Chen and C.-Y. Cheng, *Thin Solid Films*, 2012, **520**, 3054-3059.

32. P. Manivel, M. Dhakshnamoorthy, A. Balamurugan, N. Ponpandian, D. Mangalaraj and C. Viswanathan, *RSC Advances*, 2013, **3**, 14428-14437.

33. Y. Wang, Y. Li, L. Tang, J. Lu and J. Li, *Electrochemistry Communications*, 2009, **11**, 889-892.

34. Y.-C. Bai and W.-D. Zhang, *Electroanalysis*, 2010, **22**, 237-243.

35. Z. Wang, X. Zhou, J. Zhang, F. Boey and H. Zhang, *The Journal of Physical Chemistry C*, 2009, **113**, 14071-14075.

36. A. K. Chauhan, D. K. Aswal, S. P. Koiry, S. K. Gupta, J. V. Yakhmi, C. Sürgers, D. Guerin, S. Lenfant and D. Vuillaume, *Applied Physics A*, 2008, **90**, 581-589.

37. Y. Wei, L.-T. Kong, R. Yang, L. Wang, J.-H. Liu and X.-J. Huang, *Langmuir*, 2011, **27**, 10295-10301.

38. S.-X. Guo, S.-F. Zhao, A. M. Bond and J. Zhang, *Langmuir*, 2012, **28**, 5275-5285.

39. G. K. Ramesha and S. Sampath, *The Journal of Physical Chemistry C*, 2009, **113**, 7985-7989.

40. P. V. Kumar, M. Bernardi and J. C. Grossman, *ACS Nano*, 2013, **7**, 1638-1645.

41. P. Horsman, B. E. Conway and E. Yeager, *Comprehensive Treatise of Electrochemistry: Volume 7 Kinetics and Mechanisms of Electrode Processes*, Springer US, 2012.

42. A. Martínez-García, A. Sánchez-Reche and J. M. Martín-Martínez, *The Journal of Adhesion*, 2003, **79**, 525-547.

43. W. Wei, Y. Tao, W. Lv, F.-Y. Su, L. Ke, J. Li, D.-W. Wang, B. Li, F. Kang and Q.-H. Yang, *Scientific Reports*, 2014, **4**, 6289.

44. Z. Li, W. Zhang, Y. Luo, J. Yang and J. G. Hou, *Journal of the American Chemical Society*, 2009, **131**, 6320-6321.

45. J.-A. Yan and M. Y. Chou, *Physical Review B*, 2010, **82**, 125403.

46. X. Zhiping and X. Kun, *Nanotechnology*, 2010, **21**, 045704.

47. M. Dubey, I. Gouzman, S. L. Bernasek and J. Schwartz, *Langmuir*, 2006, **22**, 4649-4653.

48. M. Patel, W. Feng, K. Savaram, M. R. Khoshi, R. Huang, J. Sun, E. Rabie, C. Flach, R. Mendelsohn, E. Garfunkel and H. He, *Small*, 2015, **11**, 3358-3368.

49. G. Sobon, J. Sotor, J. Jagiello, R. Kozinski, M. Zdrojek, M. Holdynski, P. Paletko, J. Boguslawski, L. Lipinska and K. M. Abramski, *Opt. Express*, 2012, **20**, 19463-19473.

50. K. M. Sundberg, W. H. Smyrl, L. Atanasoska and R. Atanasoski, *Journal of The Electrochemical Society*, 1989, **136**, 434-439.

51. E. S. Vasquez, I. W. Chu and K. B. Walters, *Langmuir*, 2014, **30**, 6858-6866.

52. E. S. Vasquez, J. L. Cunningham, J. B. McMahan, C. L. Simpson and K. B. Walters, *Journal of Materials Chemistry B*, 2015, **3**, 6411-6419.

53. C. Malitesta, I. Losito, L. Sabbatini and P. G. Zambonin, *Journal of Electron Spectroscopy and Related Phenomena*, 1995, **76**, 629-634.

54. Y. Shao, S. Zhang, M. H. Engelhard, G. Li, G. Shao, Y. Wang, J. Liu, I. A. Aksay and Y. Lin, *Journal of Materials Chemistry*, 2010, **20**, 7491-7496.

55. A. C. Ferrari and J. Robertson, *Physical Review B*, 2000, **61**, 14095-14107.

56. K. N. Kudin, B. Ozbas, H. C. Schniepp, R. K. Prud'homme, I. A. Aksay and R. Car, *Nano Letters*, 2008, **8**, 36-41.

57. A. Eckmann, A. Felten, A. Mischchenko, L. Britnell, R. Krupke, K. S. Novoselov and C. Casiraghi, *Nano Letters*, 2012, **12**, 3925-3930.

58. D. C. Elias, R. R. Nair, T. M. G. Mohiuddin, S. V. Morozov, P. Blake, M. P. Halsall, A. C. Ferrari, D. W. Boukhvalov, M. I. Katsnelson, A. K. Geim and K. S. Novoselov, *Science*, 2009, **323**, 610-613.

59. V. C. Tung, M. J. Allen, Y. Yang and R. B. Kaner, *Nat Nano*, 2009, **4**, 25-29.

60. J. E. B. Randles, *Transactions of the Faraday Society*, 1948, **44**, 327-338.

61. M. Halik and A. Hirsch, *Adv Mater*, 2011, **23**, 2689-2695.

62. H. R. Thomas, S. P. Day, W. E. Woodruff, C. Vallés, R. J. Young, I. A. Kinloch, G. W. Morley, J. V. Hanna, N. R. Wilson and J. P. Rourke, *Chemistry of Materials*, 2013, **25**, 3580-3588.

63. M. Velický, D. F. Bradley, A. J. Cooper, E. W. Hill, I. A. Kinloch, A. Mishchenko, K. S. Novoselov, H. V. Patten, P. S. Toth, A. T. Valota, S. D. Worrall and R. A. W. Dryfe, *ACS Nano*, 2014, **8**, 10089-10100.

64. A. J. F. L. R. Bard, *Electrochemical methods : fundamentals and applications*, Wiley, New York, 1980.

65. W. Li, C. Tan, M. A. Lowe, H. D. Abruña and D. C. Ralph, *ACS Nano*, 2011, **5**, 2264-2270.

66. Y. Wu, Z. Dou, Y. Liu, G. Lv, T. Pu and X. He, *RSC Advances*, 2013, **3**, 12726-12734.

67. M. D. Hawley, S. V. Tatawawadi, S. Piekarski and R. N. Adams, *Journal of the American Chemical Society*, 1967, **89**, 447-450.

68. A. Ciszewski and G. Milczarek, *Analytical Chemistry*, 1999, **71**, 1055-1061.

Functional holey graphene oxide: a new electrochemically transformed substrate material for dopamine sensing

A.B.M. Zakaria,[a] Erick S. Vasquez,[b] Keisha B. Walters[c] and Danuta Leszczynska[d*]

Figure captions:

Fig. 1 Schematic of a 2-step electrochemical process for production of holey graphene oxide (HGO) from exfoliated graphene oxide (GO).

Fig. 2 Cyclic voltammograms for Step-1 (reduction) of GO/APTMS/GC (A) and Step-2 (oxidation) of ERGO /APTMS/GC (B) in 0.5M H_2SO_4 at 50 mV/s scan rate over the potential window from 0.0 to -1.2V and -0.2 to +1.2V vs Ag/AgCl sat.KCl, respectively [red line: first scan, black line: final scan].

Fig.3 AFM topography images collected in tapping mode for exfoliated GO (A) and HGO (B). Both samples, GO and HGO, were prepared by drop-casting dilute dispersions onto clean silicon wafers.

Fig.4 SEM images of GO/APTMS (A) and HGO/APTMS (B) on GC electrode. TEM images of exfoliated GO (C), HGO (D), and the characteristic features of immobilized β-CD on GO (E) and HGO (F), respectively.

Fig.5 XPS survey spectra (A) for GO/APTMS/GC (a), ERGO/APTMS/GC (b), and HGO/APTMS/GC (c) and C 1s high resolution spectra for GO/APTMS/GC (B), ERGO/APTMS/GC (C), and HGO/APTMS/GC (D) substrates with C1 (sp^2 C), C2 (C-O), C3 (C=O) and C4 (C-C=O or HO-C=O) peaks as indicated.

Fig.6 XPS O 1s high resolution spectra obtained for GO/APTMS/GC (A), ERGO/APTMS/GC (B) and HGO/APTMS/GC (C) showing O1 (C-O), O2 (C=O) and O3 (HO-C=O) peaks that confirms each step of the electrochemical oxidation process.

Fig. 7 FTIR transmittance spectra of GO/APTMS/GC (a), ERGO/APTMS/GC (b) and HGO/APTMS/GC (c) substrates supporting each reaction step.

Fig. 8 Raman spectra of pristine graphite (a), GO/APTMS/GC (b), ERGO/APTMS/GC (c), and HGO/APTMS/GC (d) substrates.

Fig. 9 (A) Cyclic voltammograms of 1.0 mM $Fe(CN)_6^{3-/4-}$ on GO/APTMS/GC (black), only GC (green), ERGO/APTMS/GC (blue) and HGO/APTMS/GC (red) electrodes in 1.0 M KCl at scan rate 100 mV/s; (B) Peak current values of different electrodes *versus* square root of the scan rate (mV/s).

Fig. 10 Cyclic voltammograms of 1.0 mM DA on β-CD-GO/APTMS/GC (a), β-CD-ERGO/APTMS/GC (b), HGO/APTMS/GC (c, dotted line), bare GC (d), and β-CD-HGO/APTMS/GC (e) electrodes in 0.1M PBS solution (pH 7.4) at a 50 mV/s scan rate.

Fig. 11 Current-time curve of β-CD-ERGO/APTMS/GC electrode with successive addition of DA (A) and in the absence of DA over 3600s; (B) and (C) Calibration plots illustrate a linear relationship for DA over the 0.1 to 800 µM concentration range; (D) Current responses of the modified electrode to the sequential addition of 0.05 mM DA, 0.1 mM UA, and 0.1mM AA at an applied potential of +0.200 V (vs. Ag/AgCl sat. KCl) in 0.1 M PBS solution (pH 7.4)

Tables and Scheme:

Table 1: Average C and O atomic percentages of different substrate materials based on XPS data.
Table 2: Comparative performances of different composite electrodes towards dopamine (DA) detection

Scheme 1 Mechanisms of the electrochemical behavior of DA at the modified electrode.

Fig. 1
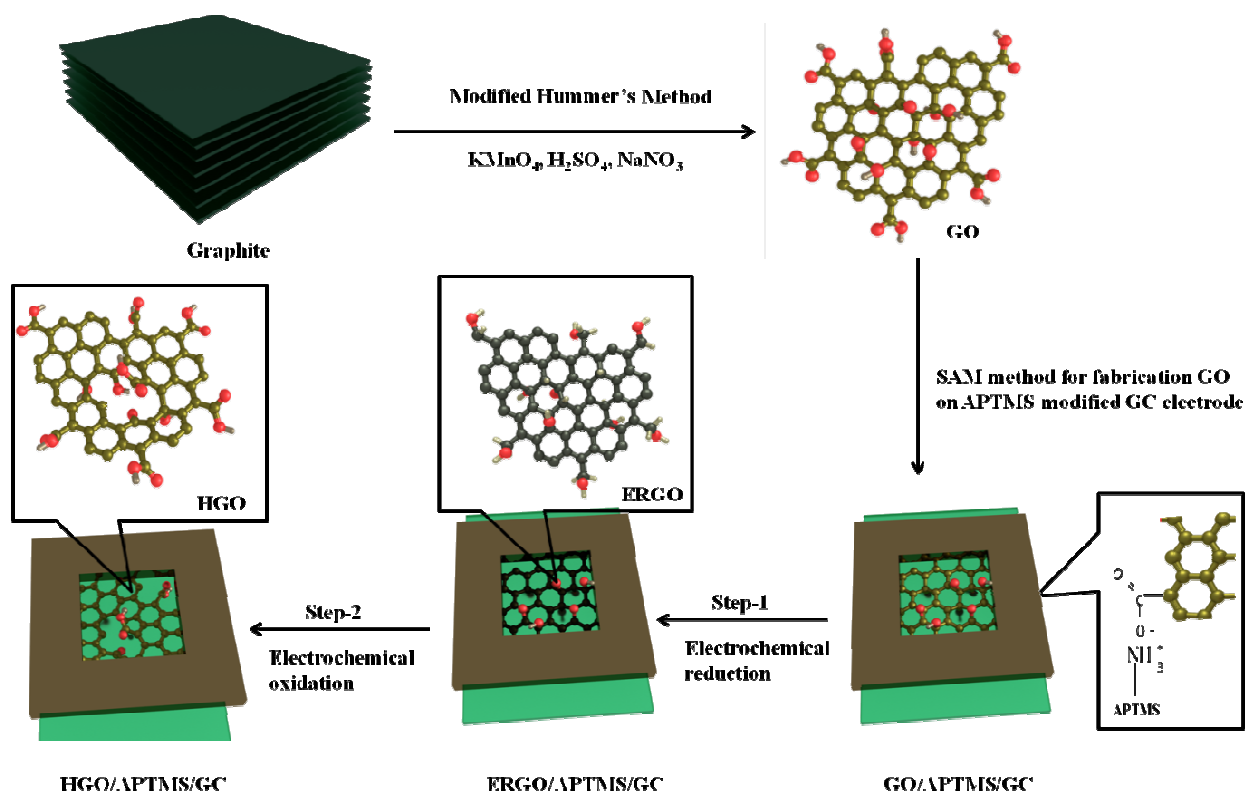
Fig. 2
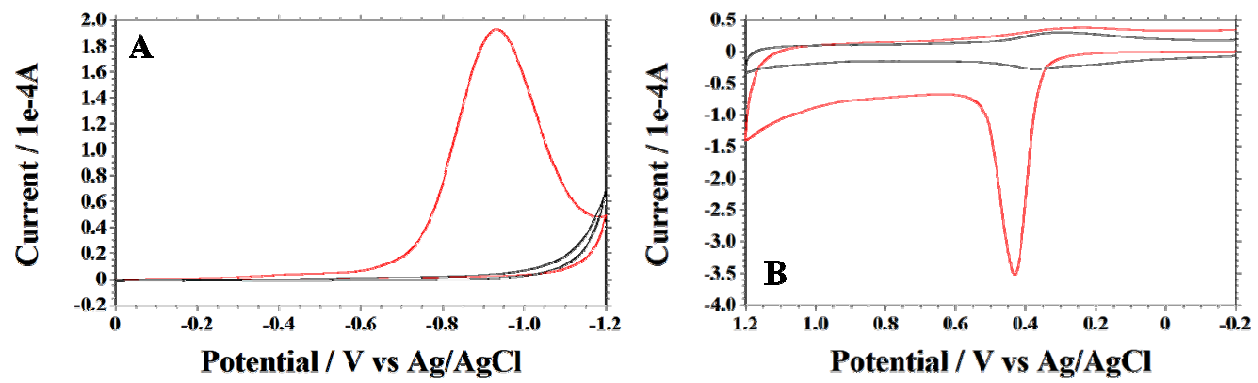
Fig. 3
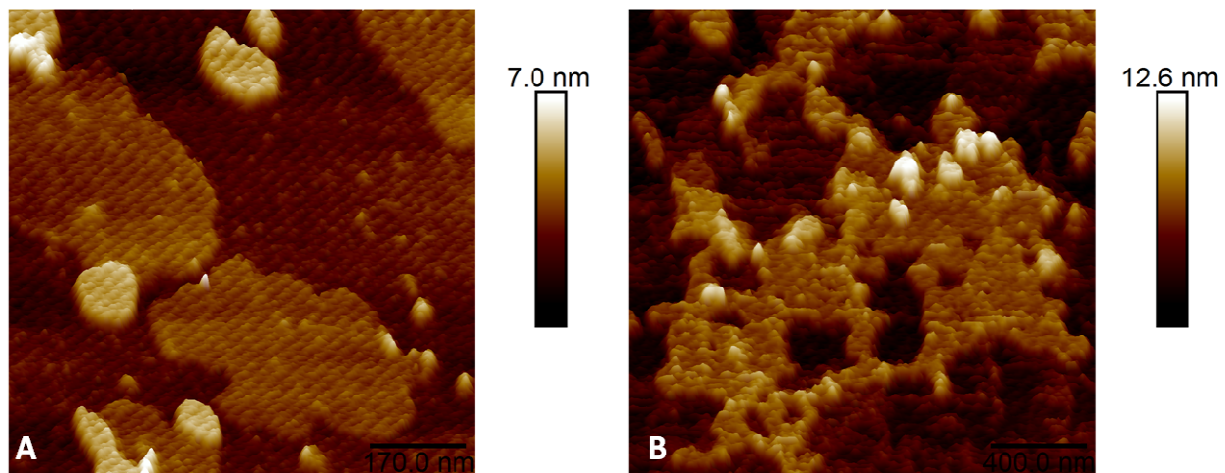
Fig. 4
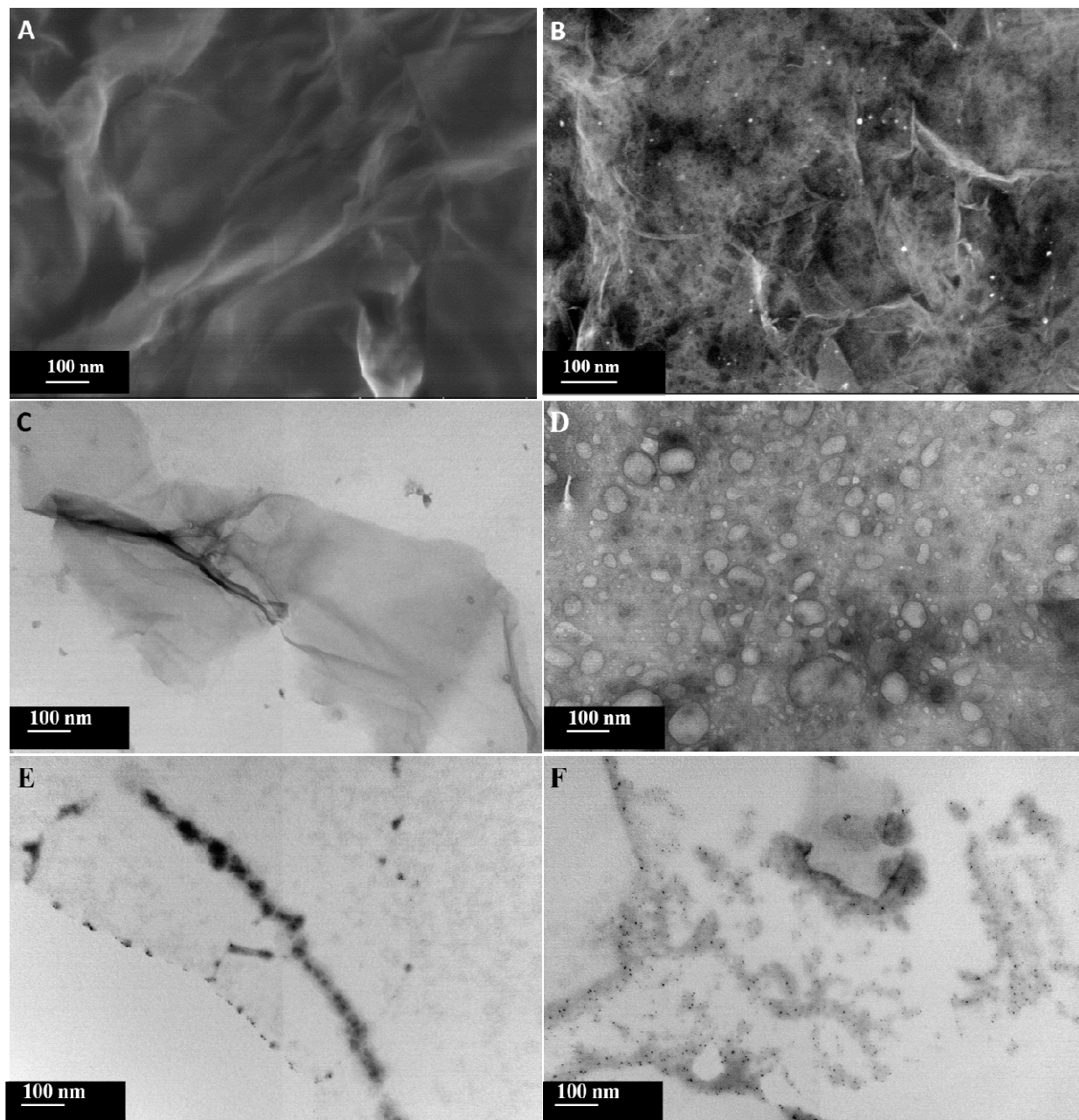
Fig. 5
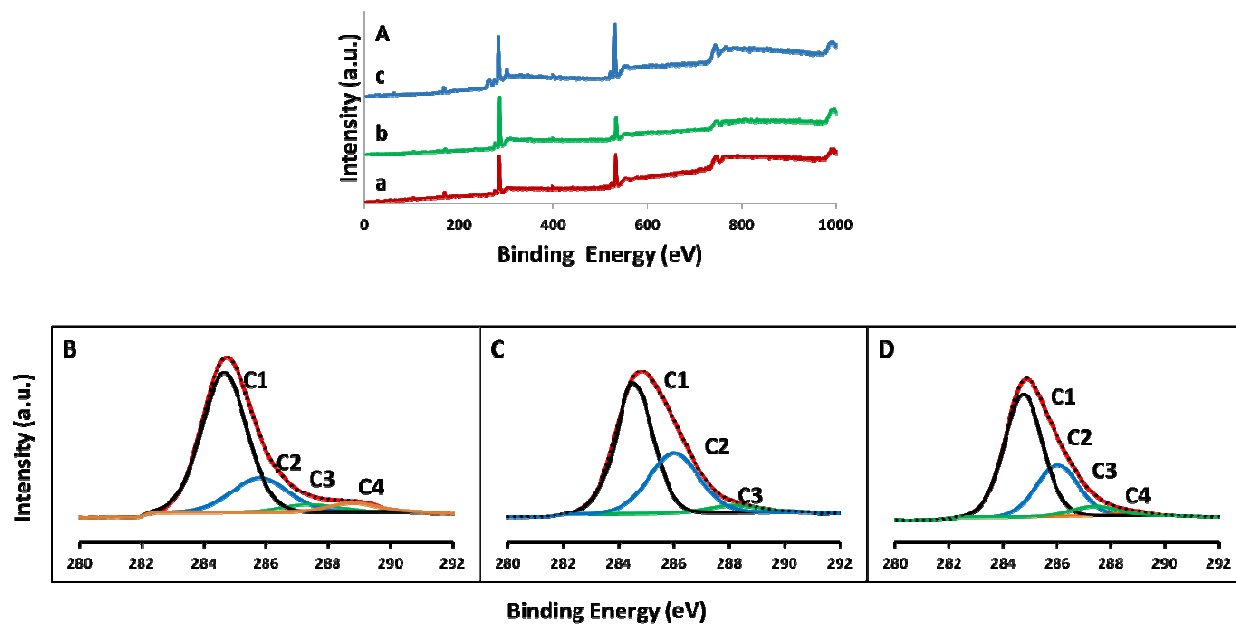
Fig. 6
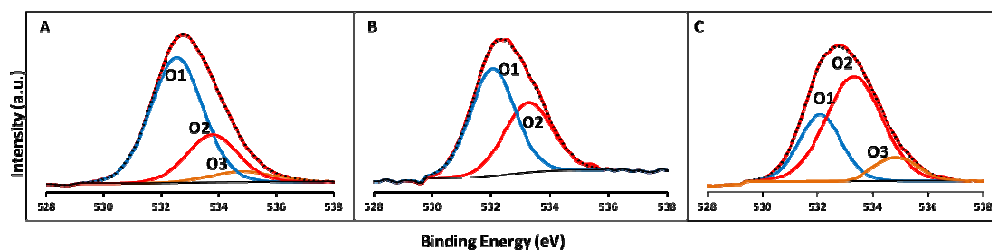
Fig. 7
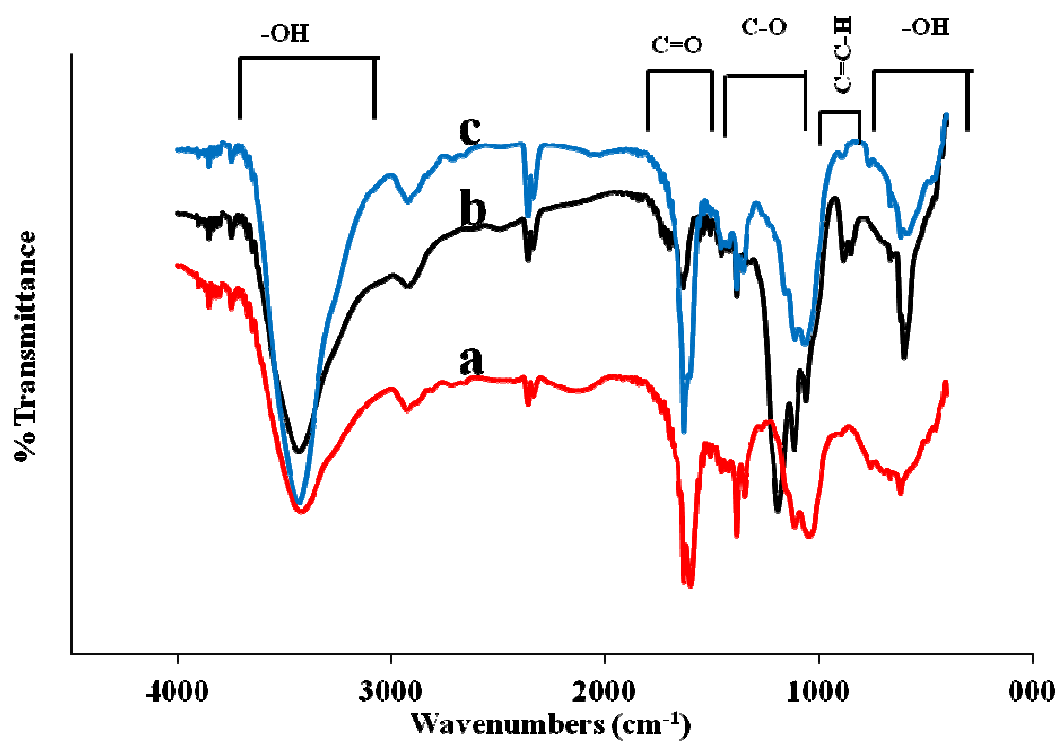
Fig. 8
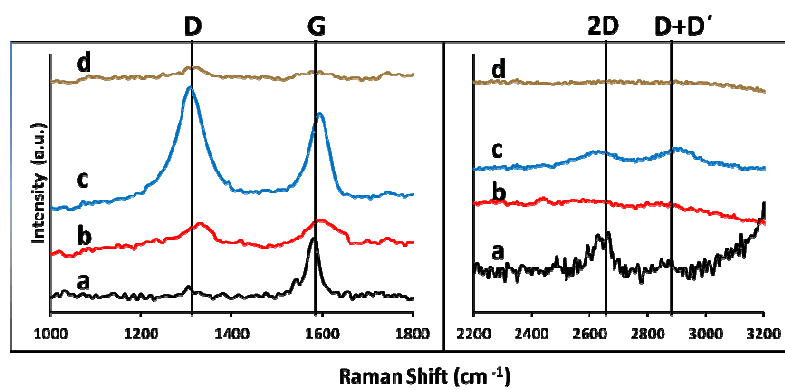
Fig. 9
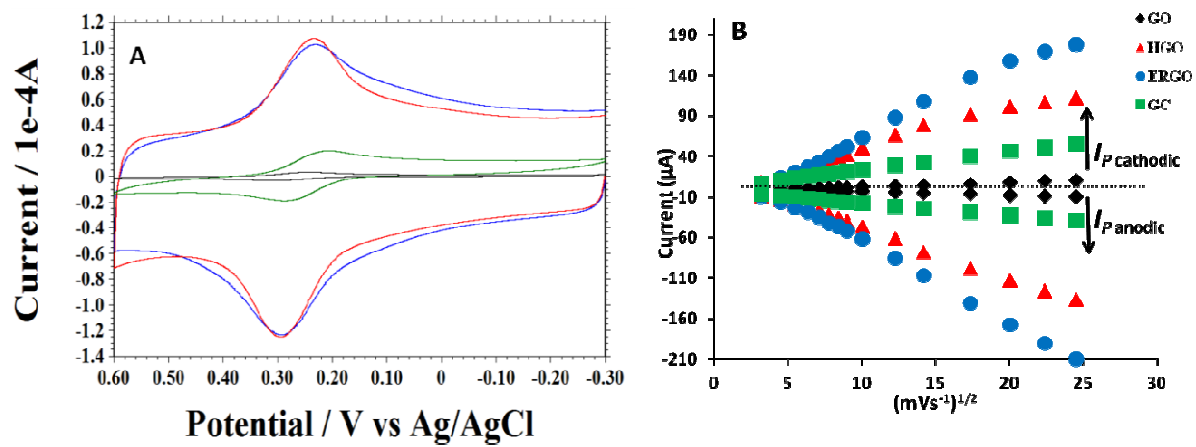
Fig. 10
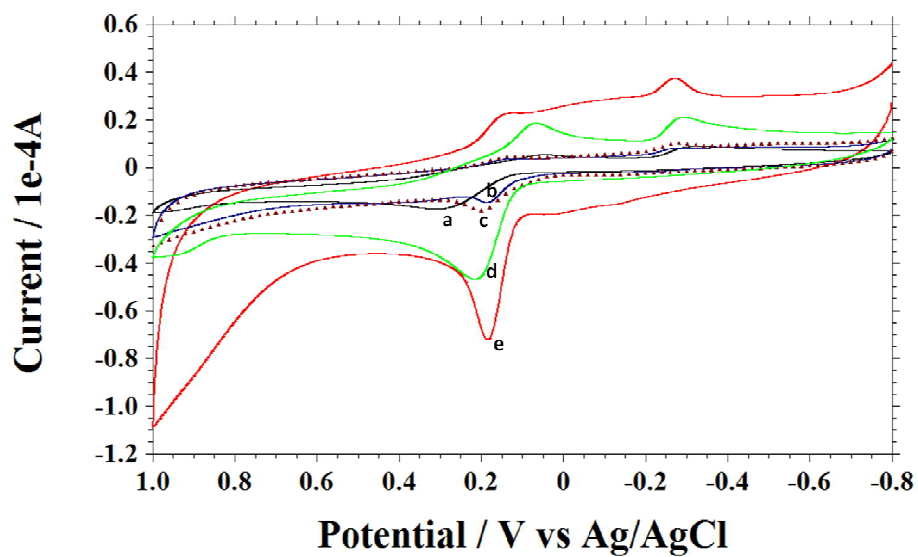
Fig. 11
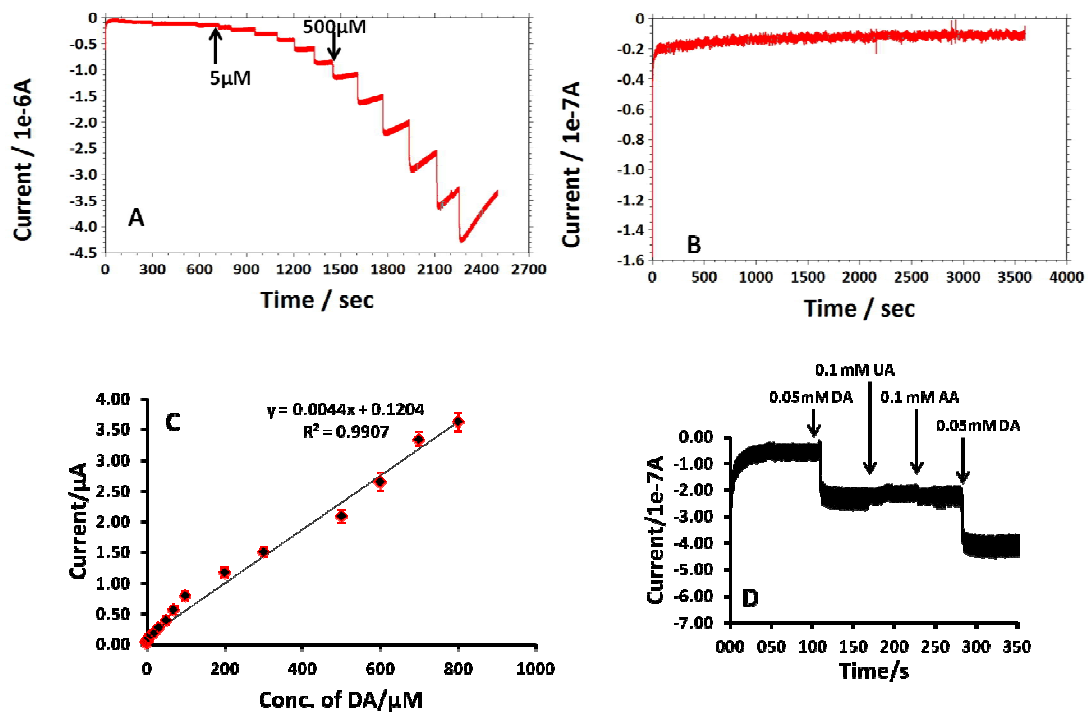
Table 1: Average C and O atomic percentages of different substrate materials based on XPS data.

Sample	C1s	O1s	C/O
Exfoliated GO only	68.2	31.8	2.14
GO/APTMS/GCE	67.6	32.4	2.09
ERGO/APTMS/GCE	80.6	19.4	4.14
HGO/APTMS/GCE	64.9	35.1	1.84

Table 2: Comparative performances of different composite electrodes towards dopamine (DA) detection.

Modified Electrode	Linear Range (μM)	Detection Limit (μM)	Reference
PA6/PAH[a]_MWCNTs/ITO	1.0-70	0.15	28
Ag-Pt/p-CNFs[b]/GCE	10.0-500	0.11	31
PEDOT/PNMPy[c]/AuNPs/GCE	1.0-100	2.0-3.0	29
Nano Pd-Au particles/GCE	0.5-6.95	0.5	32
Reduced graphene oxide/GCE	5.0-200	2.0	34
MWCNT/CPE	20 - 50	1.07	30
Pt@Au/MWNTs/GCE	10 - 120	0.08	35
PANI-GO/GCE	2.0-18	0.50	33
β-CD-HGO/APTMS/GC	0.1-800	7.6 nM	This study

[a]Polyamide 6/Poly-allylamine hydrochloride, [b] Carbon nanofibers, [c] Poly(3,4-ethylenedioxythiophene/Poly(N-methylpyrrole)
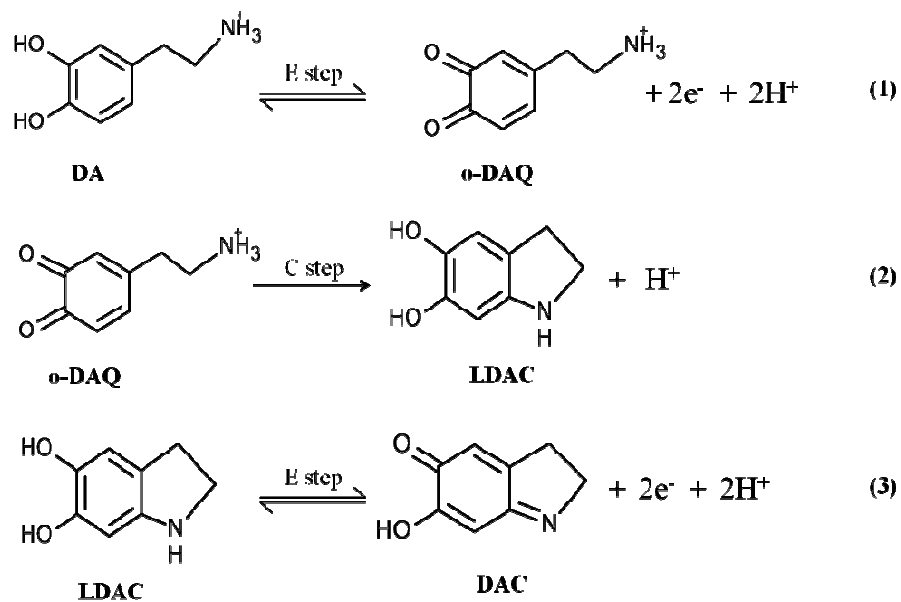
Scheme 1 Mechanisms of the electrochemical behavior of DA at the modified electrode.

277x145mm (150 x 150 DPI)